Chemical Engineering Journal 150 (2009) 572–580

Contents lists available at ScienceDirect

Chemical Engineering Journal

journal homepage: www.elsevier.com/locate/cej

Preparation and characterization of magnetite/dextran nanocomposite used as a precursor of magnetic fluid

R.Y. Hong[a,b,*], J.H. Li[a], J.M. Qu[a], L.L. Chen[a], H.Z. Li[b]

[a] College of Chemistry, Chemical Engineering and Materials Science & Key Laboratory of Organic Synthesis of Jiangsu Province, Soochow University, SIP, Suzhou 215123, China
[b] State Key Laboratory of Multi-phase Complex Systems, Institute of Process Engineering, Chinese Academy of Sciences, Beijing 100080, China

ARTICLE INFO

Article history:
Received 17 December 2008
Received in revised form 5 March 2009
Accepted 19 March 2009

Keywords:
Nanoparticle
Superparamagnetism
Magnetic fluid
Dextran
Rheological property

ABSTRACT

Magnetic nanoparticles were synthesized by the co-precipitation of Fe^{2+} and Fe^{3+} using ammonium hydroxide (NH_4OH). The obtained nanoparticles were characterized by X-ray powder diffraction, transmission electron microscopy, scanning electron microscopy, Fourier transform infrared (FT-IR) spectroscopy and vibrating sample magnetometer. In order to prepare a biocompatible water-based magnetic fluid, the nanoparticles were modified by dextran through a two-step method. The influences of dextran molecular weight on the size, morphology, coating efficiency and magnetic property of magnetite/dextran nanocomposite were investigated. The magnetite/dextran nanocomposite was dispersed in water to form a magnetic fluid by ball milling. The rheological property of magnetic fluids was investigated using a rotating rheometer.

1. Introduction

In the last decade, nanotechnology has quickly developed and has become an important aspect in the fields of biomedicine and diagnostics [1–4]. Among inorganic materials, magnetic nanoparticles (magnetite nanoparticles or maghemite nanoparticles, MNPs) with a diameter of about 5–20 nm have attracted much attention. Since the biocompatibility of the MNPs has already been proven [5], their applications in biomedicine, such as: (a) cellular therapy in cell labeling, separation and purification [6]; (b) protein immobilization [7]; (c) contrasting enhancement in magnetic resonance imaging (MRI) [8]; (d) localized therapeutic hyperthermia [9]; (e) biosensors [10], etc., become increasingly wide and deep in recent years.

In these applications, the MNPs must possess superparamagnetism, high saturation magnetization, extra anisotropy contributions, high dispersibility and biocompatibility. Superparamagnetic particles are of great interest to researchers, because the particles do not display any overall magnetism after removal of external magnetic field [11]. In addition, van der Waals force and magnetic force among MNPs will lead to aggregation. Therefore, the surface modification of nanoparticles is indispensable and the particle surface should be modified using inorganic [12,13] or organic materials [14–18]. Though the application of MNPs has been put into practice for many years both in vitro and in vivo diagnostics [19], studies on the surface modification of MNPs are still significant.

Coating organic polymers on the surface of MNPs endows the particles some important properties that the bare particles lack. Polymer coating could enhance the compatibility between nanoparticles and aqueous medium, prevent particles from oxidation, reduce toxicity, extend storage life and facilitate transport, etc. Polymers for coating can be classified into natural and synthetic substances. Natural polymers include dextran, chitosan, gelatin, etc. Synthetic polymers include poly (ethyleneglycol) (PEG), poly (vinylpyrrolidone) (PVP), poly (vinyl alcohol) (PVA) and polyacrylic acid (PAA), etc. Dextran as natural polysaccharide, which is widely used in the pharmaceutical field, has attracted much attention. Dextran is water soluble, inert in biological systems and does not influence cell viability [20]. In some research groups, magnetite/dextran nanocomposite was prepared by a one-step method, in which dextran was linked with MNPs through van der Waals force and hydrogen bond. In this case, when magnetic fluid is injected into veins, the magnetic fluid will be diluted, leading to the precipitation of the magnetic nanoparticles. In order to resolve the problem, a two-step method was proposed in the present investigation to bond dextran onto the surface of MNPs through chemical linkage.

Control of the rheological property of magnetic fluids (MFs) is very important during their applications [21–28]. Under an applied magnetic field, these particles acquired an induced dipole moment causing the particles to aggregate. The rheological property of MF

* Corresponding author at: College of Chemistry, Chemical Engineering and Materials Science, Soochow University, SIP, Suzhou 215123, China.
Tel.: +86 512 6588 0402; fax: +86 512 6588 0089.
E-mail address: rhong@suda.edu.cn (R.Y. Hong).

1385-8947/$ – see front matter © 2009 Elsevier B.V. All rights reserved.
doi:10.1016/j.cej.2009.03.034

Nomenclature

C_s	solid content of MF (g)
H_0	intensity of magnetic field (mT)
k	consistency index of Herschel–Bulkley model (kg s^{2n}/m)
l	length of surfactant chain (m)
n	shear-thinning exponent
r	radius of an aggregate (m)
r_0	radius of a primary particle (m)
R	distance between two particles (m)

Greek letters

χ	susceptibility of MNPs (m^3/g)
δ	distance between MNPs (m)
γ	shear rate (rps)
η	viscosity (Pa s)
η_c	Carson's viscosity (Pa s)
μ^0	susceptibility of vacuum
ρ_s	density of MNPs (g/$cm^{3)}$
τ_0	yield stress (Pa)
τ_c	Carson's yield stress (Pa)
τ	shear stress (Pa)
τ_{H_0}	yield stress of MFs under applied magnetic field (Pa)

is influenced by the type and dosage of surfactants, the intensity of external magnetic field and the concentration of solid particles. In our previous study, the rheological behavior of bilayer surfactant stabilized MF [29] with and without external magnetic fields was described using the Bingham, Carson or Herschel–Bulkley models, and suitble constitutive equations for shear stress and yield stress threshold were proposed [30].

In this paper, superparamagnetic MNPs were prepared by co-precipitation and were surface modified by dextran via chemical bond. The magnetite/dextran nanocomposite was dispersed in water to form MF. The influences of surfactants, magnetic field intensity and solid content on the rheological property of MF were investigated using a rotating rheometer.

2. Experimental

2.1. Materials

Iron (III) chloride hexahydrate ($FeCl_3{\cdot}6H_2O$), iron (II) sulfate heptahydrate ($FeSO_4{\cdot}7H_2O$), aqueous ammonia (25%), dextran with molecule weight of 3000, 10,000, 20,000 and 40,000 (marked as T3, T10, T20 and T40, respectively), and 3-aminopropyltriethoxysilane (APTES) were employed. In all experiments, deionized water was used.

Aldehyde dextran was prepared using sodium periodate as reported by Betancor et al. [31], and the reaction equation is shown in Fig. 1. 3.33 g of dextran was dissolved in 100 mL of deionized water. 8 g of sodium periodate ($NaIO_4$) was added, and the mixture was stirred for 3 h in the dark at 25 °C. After reaction, purification was performed by dialysis for 24 h to remove the formic acid produced in the process of oxidation. The deionized water used in the dialysis process was replaced every 4 h.

2.2. Preparation of magnetic nanoparticles

MNPs were prepared according to the method described previously [32]. A mixed solution of $FeCl_3$ (0.5 M) and $FeSO_4$ (0.5 M) with a molar ratio of 1.75:1 was sonicated for 30 min at room temperature, and then some dosage of ammonia solution was quickly poured into the mixture with vigorous stirring under argon protection, followed by slowly dropping additional ammonia solution until the pH of the solution reached 9. Afterward, the solution was stirred for 30 min in argon atmosphere and aged for 24 h. Finally, the black precipitate was washed with deionized water and collected by a magnet for several times, and dried under vacuum for 24 h.

2.3. Nanoparticles modified with amino-silane

6.0 mL of APTES ($NH_2(CH_2)_3Si(OCH_2CH_3)_3$), 1.0 g of the MNPs and 50 mL of ethanol were added in a 250 mL three-necked round-bottom flask. Under argon protection, the mixture was stirred for 5 h at 60 °C. After cooling to room temperature, the product was washed with deionized water and methanol for several times, and dried in vacuum at room temperature. After the above treatment, the MNPs were modified with amino-silane. The reaction mechanism was illustrated in Fig. 2.

2.4. Dextran-coated magnetic nanoparticles

1.0 g of aminated MNPs was dispersed in 50 mL of aldehyde dextran solution in the argon atmosphere. The pH of the suspension was adjusted to 3 with hydrochloric acid, and the reaction was sustained at 60 °C for 24 h. Then, the pH was adjusted to 9 using ammonia solution, and the suspension was allowed to react continuously for 4 h at 60 °C. The produced Schiff's base was reduced by adding 0.6 g of sodium borohydride at pH 9 in the dark for 24 h. After centrifuging and washing with abundant deionized water, the dextran-coated MNPs were obtained.

2.5. Preparation of magnetic fluid

The obtained magnetite/dextran MNPs were dispersed in deionized water by ball milling at 40 rpm for 3 h at room temperature to prepare MF with different solid contents. The ball milling was performed using a high-energy ball mill under sealing. The pots and balls were made of agate.

2.6. Characterization

A conventional 2,4-dinitrophenylhydrazine method was introduced to detect the aldehyde constituent after periodate oxidation of dextran [33]. The procedure was described as follows: 3 mL of sulfuric acid (0.3 mL) and ethanol (0.95 wt.%, 2.7 mL) mixted solution was prepared. Fresh 2,4-dinitrophenylhydrazine solution was prepared by dissolving 0.04 g of 2,4-dinitrophenylhydrazine into the mixted solution, and the obtained solution was diluted to 10 mL with water and filtered. Some dextran aldehyde was added into 2 mL of newly prepared 2,4-dinitrophenylhydrazine solution, and the mixture was stirred for some time.

The efficiency of dextran oxidation was measured by testing the released formic acid [34]. When the oxidation of dextran was finished, we sampled 25 mL of the solution and added 2 mL of ethylene glycol to destroy excessive periodate. After some time, the released formic acid was titrated with NaOH solution (0.1 M) using an end-point titration method.

The functional groups of all samples were identified by a Nicolet Avatar 360 Fourier transform infrared (FT-IR) spectroscopy. Measurements were performed with pressed pellets that were made using KBr powder as diluent. The FT-IR spectrum was collected between the wavenumber of 400 cm^{-1} and 4000 cm^{-1}.

The bare and dextran-coated MNPs were characterized by X-ray diffraction (XRD) (D/Max-IIIC, Japan) using Cu-kα radiation (λ = 1.5406 Å). The crystal structure of the MNPs was determined according to the JCDPS 5-0664 of International Center for Diffraction Data.

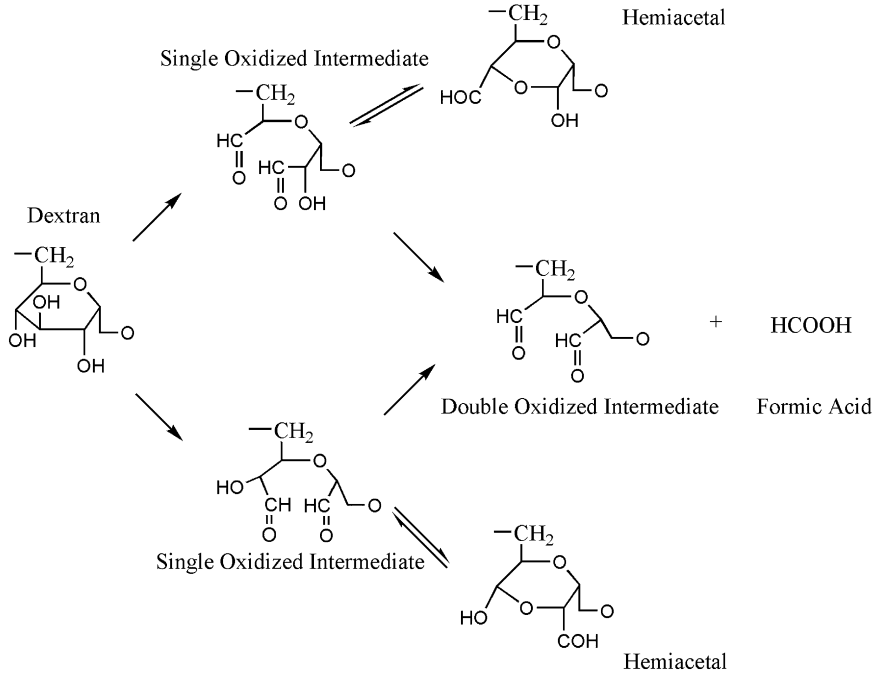

Fig. 1. Reaction equation of hydrazine reagent with aldehyde.

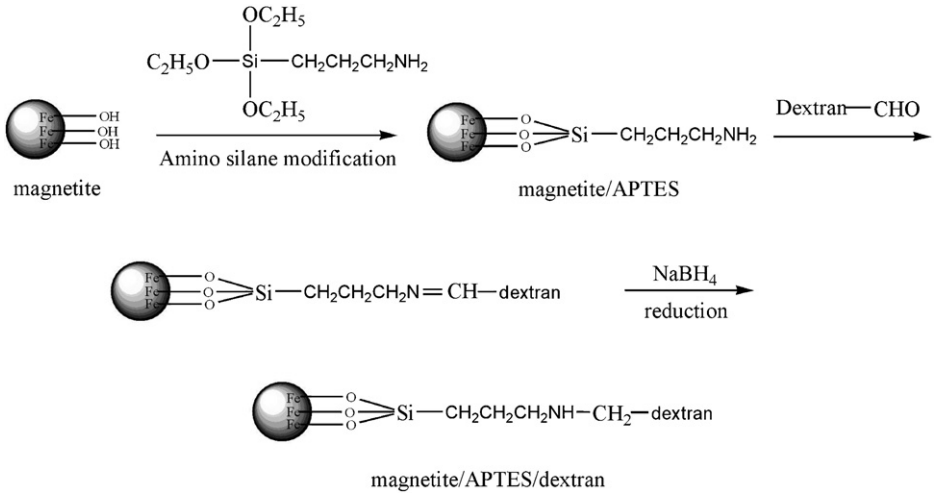

Fig. 2. Synthesis route for the dextran-coated magnetite nanoparticle.

The surface of the bare and dextran-coated MNPs was observed with field emission scanning electron microscope (SEM, Hitachi S-570). The inner morphology of the two kinds of MNPs was determined by transmission electron microscope (TEM, Hitachi H-600-II) with an acceleration voltage of 200 kV.

The size of particles/aggregates suspended in MF was determined by Malvern HPPS5001 dynamic light scattering meter with the scanning range of 0.6–6000 nm. The samples were dispersed in water completely with sonicate before measurement.

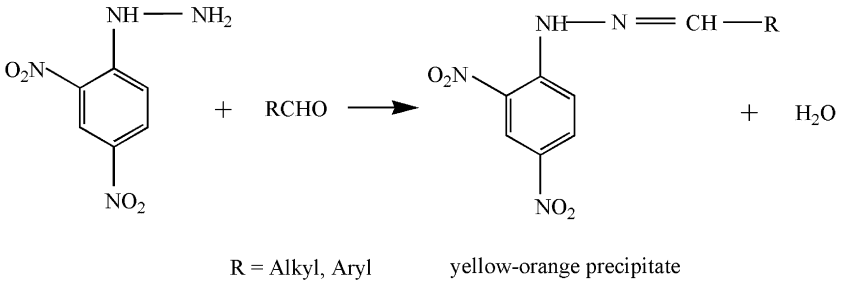

Fig. 3. Periodate oxidation of dextran.

PerkinElmer TGA-7 was employed to perform the thermogravimetric analysis (TGA). Dried samples (1–5 mg) were placed in the TGA furnace and the measurements were carried out under nitrogen with a heating rate of 20 °C/min from 50 °C to 700 °C.

Measurement of magnetic property was performed using a HH-15 vibrating sample magnetometer (VSM, I_{max} = 50 A, P ≤ 6 kW, H_{max} = 1500 Oe, sensibility between 4–5 × 10^{-5}).

The rheological property measurement of MF was carried out using a rotating rheometer (LV DV-III+, Brookfield, USA). The rotating speed range is 0.01–250 rpm, while the viscosity range is from 1 cP to 2 McP. Water with constant temperature supplied by a thermostatic chamber was used to control the temperature during measurements. The control precision of temperature can be achieved to ±0.1 °C. The spindle of rotating rheometer was chosen according to the viscosity range of MF, normally within 30–70% of the maximum torque. The torque during subsequent experiments was all kept within this range. A large cone spindle (CPE-40, with a diameter of 48 mm and a cone angle of 0.8°) and a small one for low and high viscosity (CPE-52, with a diameter of 24 mm and an angle of 3°) suspensions, respectively, were employed in the measurements. The volume of the sample used in each test was 0.5 mL.

3. Results and discussion

3.1. Aldehyde constituent

Hydrazine reagent is one of the most important organic qualitative reagents for the detection of aldehyde in liquid samples. In numerous hydrazine reagents, 2,4-dinitrophenylhydrazine has been used as a standard reagent. 2,4-dinitrophenylhydrazine reacts with aldehyde compounds to form the hydrazone compound, as presented in Fig. 3. Because the oxidation process produces dextran aldehyde, a clear yellow-orange precipitate was observed. An experiment for comparison was also carried out with the same conditions for dextran without oxidation, and no precipitate was observed. The phenomenon demonstrated the formation of aldehyde in the oxidation of dextran.

The percent of dextran oxidation was determined using NaOH titration method. By calculation, it is found that oxidation percent of dextran is 100%, which is also proved by a published article [35].

3.2. FT-IR spectra

The FT-IR spectra of different samples are illustrated in Fig. 4. From the spectrum of Fe_3O_4 in Fig. 4a, one can find the characteristic absorption peaks of Fe–O bond at about 416.8 cm^{-1} and 563.4 cm^{-1}. The broad absorption peak at about 3195.1 cm^{-1} can be ascribed to hydroxyls, which are originated from the water adsorbed on the surface of MNPs [36]. The spectrum of Fe_3O_4 nanoparticles treated by APTES (Fig. 4b) exhibits absorptions at 3401.3 cm^{-1}, 2860 cm^{-1}, 1114.1 cm^{-1} and 1009.0 cm^{-1}, which are characteristic peaks of the stretching vibration of —NH—, —CH_2—, Si—O—C and Fe—O—Si, respectively [8]. It indicates that the coupling agent APTES has been grafted onto the MNPs' surface. The reaction mechanism is illustrated in Fig. 2. In Fig. 4c, one can find the characteristic absorption peak of C—N stretching vibration at 1032.1 cm^{-1}, implying that dextran (T20) has been grafted onto the surface of MNPs [37].

3.3. X-ray diffraction

X-ray powder diffraction pattern of Fe_3O_4 nanoparticles is illustrated in Fig. 5a. It is found that there are a series of characteristic peaks: 2.964 (2 2 0), 2.525 (3 1 1), 2.092 (4 0 0), 1.717 (4 2 2), 1.612 (5 1 1), 1.478 (4 4 0) and 1.276 (5 3 3), which are well indexed to the cubic inverse spinel structure of Fe_3O_4 crystal. The average crystallite size D could be obtained using the Debye–Sherrer formula $D = K\lambda/(\beta \cos\theta)$, where K is Sherrer constant, λ the X-ray wavelength, β the peak width of half-maximum, and θ is the Bragg diffraction angle [32]. The crystallite size is calculated to be about

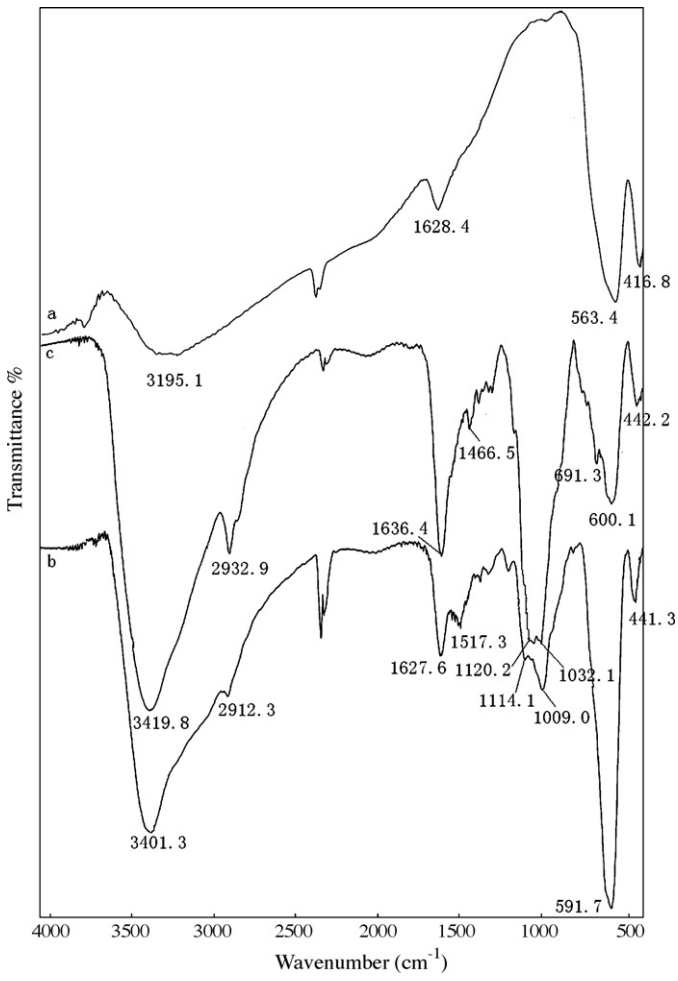

Fig. 4. FT-IR spectra of Fe_3O_4 nanoparticles (a), Fe_3O_4 nanoparticles treated by APTES (b) and Fe_3O_4 nanoparticles modified by dextran (T20) (c).

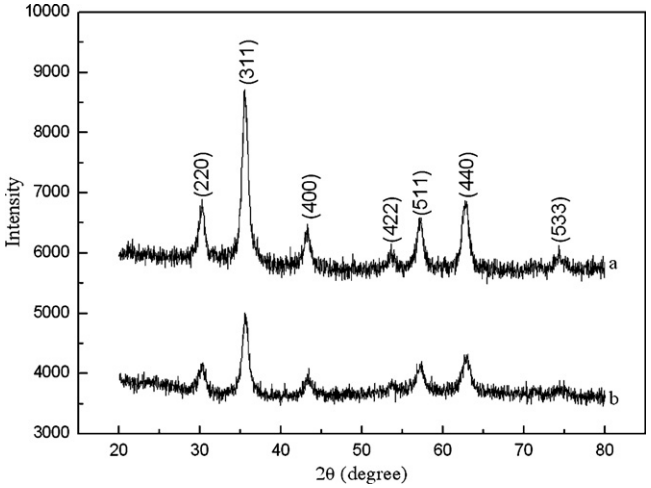

Fig. 5. XRD pattern of (a) Fe_3O_4 nanoparticles; (b) dextran-coated (T20) Fe_3O_4 nanoparticles.

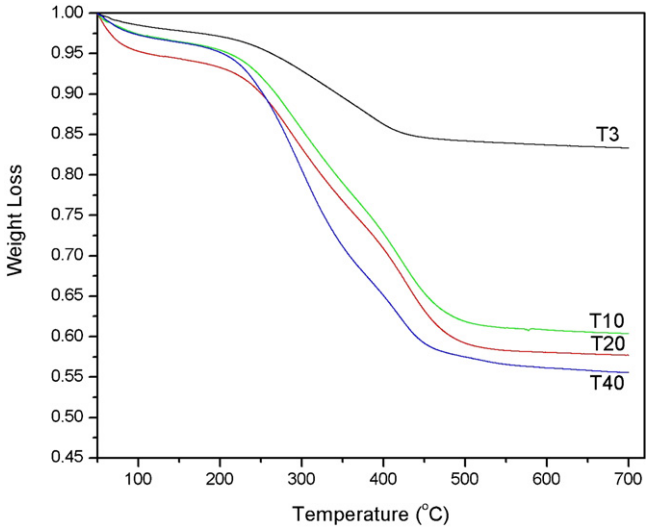

Fig. 6. Relationship between weight loss and different molecular weight dextran.

19 nm. Fig. 5b shows the XRD pattern of dextran-coated (T20) MNPs, demonstrating that the crystal structure of MNPs does not change after surface modification.

3.4. Thermal analysis

In general, TGA illuminates the relative composition of magnetite core, dextran shell and solvent leftover (or water). Fig. 6 shows weight loss curves of magnetite/dextran nanocomposites obtained using a thermogravimetric (TG) analyzer. Because the TG was performed under N_2 atmosphere, the oxidation of magnetite was greatly reduced. In the thermogram, two stages of weight loss are observed. The first weight loss stage (below 130 °C) can be ascribed to the evaporation of water molecules in the polymer matrix, while the other stage beginning at about 220 °C is due to the decomposition of dextran [8]. From the thermogram, we can calculate the coating efficiency of dextran with different molecular weight (see Table 1) and the weight ratio of iron to dextran. The results indicate that there is more dextran participated in the formation of magnetite/dextran nanocomposite with the increase of molecular weight of dextran. Obviously, the reason is that the dextran with high molecular weight has more chance to react with magnetite/amino-silane. However, with the further increase of molecular weight, the dextran chains are tangled around the nanoparticles, so the coating efficiency changes slightly.

3.5. Scanning and transmission electron microscopy

Fig. 7 shows the SEM images of bare and modified MNPs after the drying of diluted MF. Comparing the two micrographs, one can find that the aggregation remains even after the coating of the dextan (T20).

Fig. 8 illustrates the TEM images of the two kinds of nanoparticles after drying. Fig. 8a shows that most of the bare Fe_3O_4 nanoparticles are quasi-spherical and their diameter is about 20 nm, in accordance with the result of X-ray diffraction analysis. Due to large specific surface area and high surface energy, some nanoparticles aggregate. Fig. 8b shows the TEM image of the surface modified MNPs, and one can find that aggregation is almost the same, resulting from the intertwisting of the coated dextran (T20) [38].

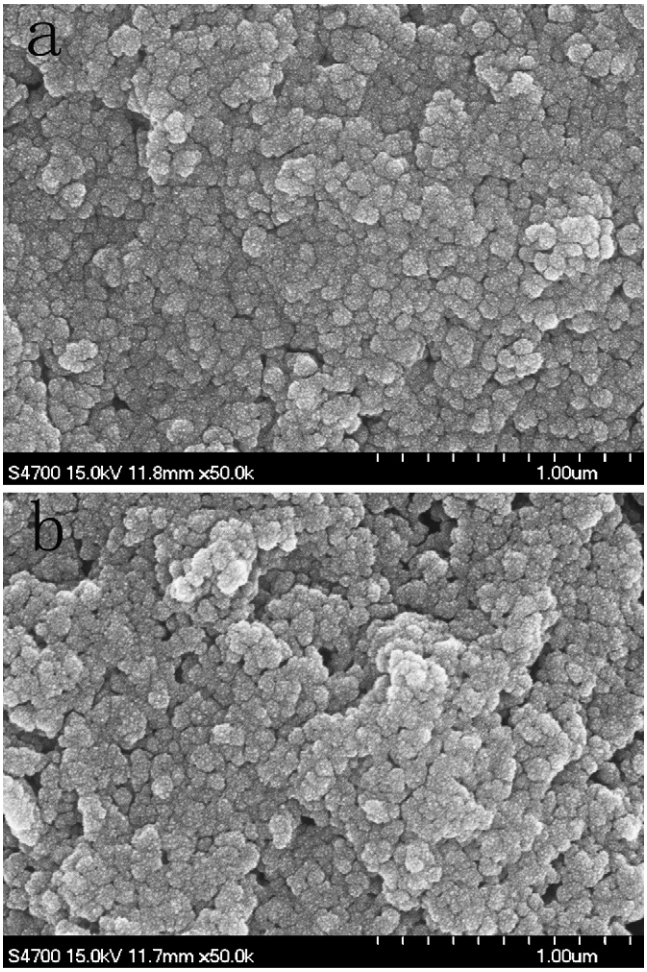

Fig. 7. SEM of (a) Fe_3O_4 nanoparticles; (b) dextran-coated (T20) Fe_3O_4 nanoparticles.

3.6. Particle size distribution

From Table 2, one can see that the mean size of nanocomposite increases gradually with the increasing dextran molecular weight. This phenomenon illuminates that the larger the molecular weight of dextran, the thicker the coating layer. Besides, one can also find that the size of nanocomposites obtained by dynamic light scattering is much larger than that obtained by TEM. This can be explained that MNPs do not exist as individual particles and some primary particles aggregate due to the magnetism of nanoparticles and the entanglement of long chains of dextran [38].

Table 1
Coating percentage and weight ratio of iron (II and III) to dextran.

Molecular weight of dextran	Coating percentage	Weight ratio of iron to dextran
T3	16.2%	1:0.270
T10	38.2%	1:0.850
T20	41.8%	1:0.990
T40	44.3%	1:1.10

Table 2
Size distribution of magnetite/dextran nanocomposite. The size distribution was measured using a Malvern HPPS5001 dynamic light scattering meter.

Sample	Fe_3O_4/T3	Fe_3O_4/T10	Fe_3O_4/T20	Fe_3O_4/T40
$d(0.99)_{num}$ (nm)	77.80	121.4	156.2	192.1

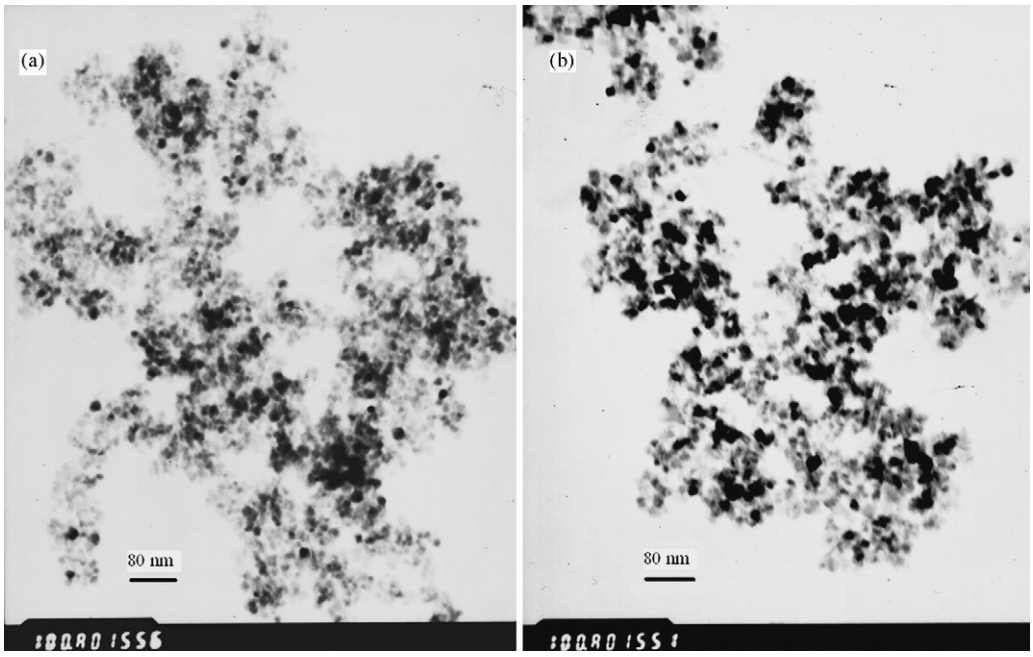

Fig. 8. TEM of (a) Fe_3O_4 nanoparticles; (b) dextran-coated (T20) Fe_3O_4 nanoparticles.

3.7. Magnetic property

The hysteresis loops of bare and dextran-coated MNPs are shown in Fig. 9. The two kinds of MNPs demonstrate superparamagnetism, while the saturation magnetization of the magnetite/dextran MNPs nanocomposite is lower than that of bare MNPs. The reduction of saturation magnetization is due to the nonmagnetic coating layer. It is found in Fig. 9 that the saturation magnetization of all samples is above 20 emu/g. Moreover, with the increase of the molecular weight of dextran, the saturation magnetization becomes smaller. This could be explained that the higher the coating efficiency, the lower the MNPs content.

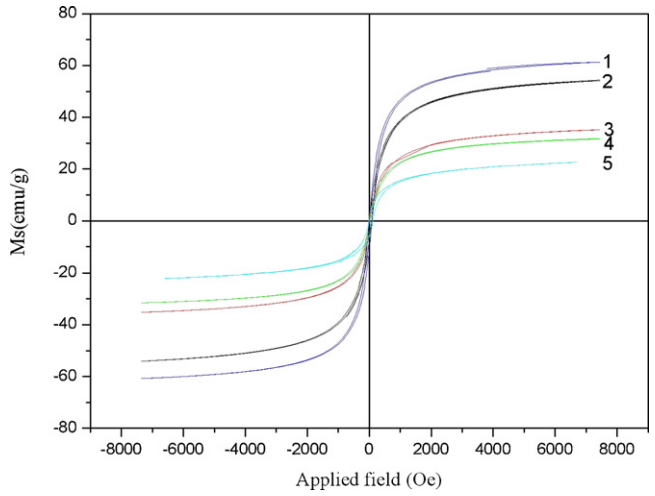

Fig. 9. Magnetic hysteresis loops for magnetite nanoparticles and magnetite/dextran nanocomposites, (1) Fe_3O_4, (2) Fe_3O_4/T3, (3) Fe_3O_4/T10, (4) Fe_3O_4/T20, (5) Fe_3O_4/T40.

Table 3
Analyzed results using Bingham model of MF with dextran (T20) without magnetic field.

Solid content, c_s (wt.%)	5	10	15	25	35
Viscosity, η_0 (mPa s)	2.2	5.20	8.1	10.3	21
Yield stress, τ_0 (Pa)	1.6	3.5	0.0	−0.33	−1.1
Correlation coefficient (%)	97.7	97.4	97.6	97.5	89.3

Table 4
Analyzed results using Carson model of MF with dextran (T20) without magnetic field.

Solid content, c_s (wt.%)	5.00	10.0	15.0	25.0	35.0
Carson's viscosity, η_c (mPa s)	2.14	4.80	8.18	10.3	23.8
Carson's yield stress, τ_c (Pa)	0.0	0.300	0.0	0.0	1.80
Correlation coefficient (%)	99.3	99.4	98.9	98.7	97.5

3.8. Rheological property of magnetic fluid

Based on the unique magnetic property and biocompatibility, MNPs offer a high potential for several biomedical applications,

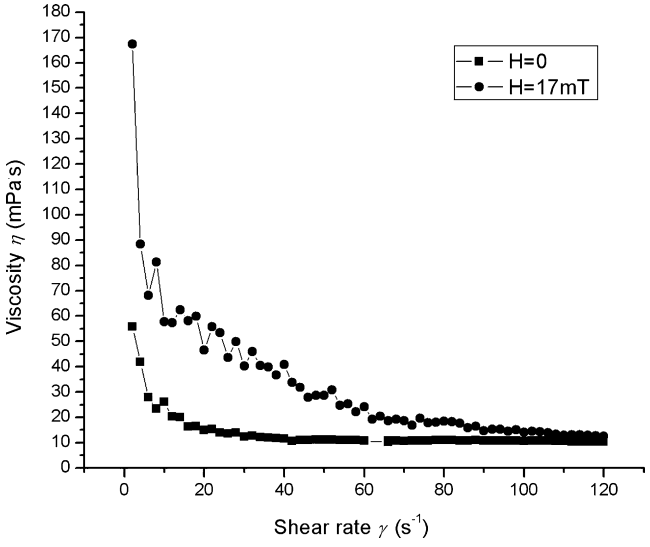

Fig. 10. Viscosity versus shear rate of MF (stabilized by T20 dextran) with and without magnetic field (T = 23.5 °C).

Table 5
Analyzed results using Herschel–Bulkley model of MF with dextran (T20) without magnetic field.

Solid content, c_s (wt.%)	5.00	10.0	15.0	25.0	35.0
Herschel–Bulkley coefficient, k (kg s^{n-2}/m)	3.22	6.30	7.50	9.54	14.3
Yield stress, τ_0 (Pa)	0.0	0.200	0.310	0.420	0.530
n	0.940	0.970	1.00	1.03	1.08
Correlation coefficient (%)	100	100	99.9	100	99.9

such as drug targeting, magnetic cell separation, magnetic hyperthermia and enzyme immobilization. The applications are based on the magnetic fluid, which could be easily injected into the body via subcutaneous or intravenous injection. After injection, a magnet is usually applied to concentrate the magnetic fluid around an affected part of the body. Therefore, high magnetism and proper fluid stabilization are required for the biomedical applications. It is necessary to investigate the rheological behavior of magnetic fluid with or without an external magnetic field.

3.8.1. Viscosity under magnetic field

The MNPs were coated with the dextran (T20), and the prepared MF has the solid content of 20%. A magnetic field with the intensity of H = 17 mT was applied between the spindle and cup of the rotating rheometer. The intensity of magnetic field was measured using a Hall-effect sensor. The viscosity of MF with and without magnetic field was illustrated in Fig. 10, showing that the external magnetic field has obvious effect on the viscosity of MF. The reason is that: the viscosity of water is determined by the interaction among water molecules. For water-based MF, the viscosity is determined by the viscosity of water and the interaction among MNPs and surfactants. The external magnetic field enhances the interaction among MNPs, therefore, the viscosity of MF increases under magnetic field. On the other hand, the external magnetic field can also rearrange the MNPs, leading to the formation of orderly microstructures. As the shear rate increases, the microstructures are destroyed under the shear stress. Thus, the viscosity of MF with external magnetic field descends more rapidly with the increasing shear rate.

3.8.2. Constitutive equations with and without an external magnetic field

There are three kinds of rheological models for suspensions that are usually used: (1) The Bingham model, taking account of the yield stress of fluids, adopts the following form, $\tau = \tau_0 + \eta\gamma$. (2) The Carson model, taking account of both the yield stress and the shear-thinning behavior, uses the form, $\sqrt{\tau} = \sqrt{\tau_c} + \sqrt{\eta_c\gamma}$. (3) The Herschel–Bulkley model also takes account of both the yield stress and the shear-thinning. This model usually can be simplified as: $\tau = \tau_0 + k\gamma^n$ and $\eta = k\gamma^{n-1}$, where, τ_0 is yield stress, k consistency index and η is viscosity. That is to say, when $\tau < \tau_0$, the material remains rigid; otherwise, the material flows as a power-law fluid.

For MF, when the shear rate is low, the disordered arrangement of MNPs increases the resistance of flow, so the fluidity of MF is reduced. When the shear rate increases, MNPs begin to arrange their orientation along with the shearing direction. This kind of arrangement leads to the decrease of viscosity. The three rheological models are used to describe the rheological property of highly concentrated MF with and without an external magnetic field. By correlating the experimental results using the software provided by the Brookfield (Brookfield, 2006), the model parameters of the three constitutive equations are obtained, as listed in Tables 3–8.

Table 6
Analyzed results using Bingham model of MF with dextran (T20), H = 17 mT.

Solid content, c_s (wt.%)	5.00	10.0	15.0	25.0	35.0
Viscosity, η_0 (mPa s)	1.45	2.40	2.57	8.34	16.5
Yield stress, τ_0 (Pa)	5.35	7.10	5.68	5.61	4.53
Correlation coefficient (%)	80.7	83.3	81.8	91.9	80.3

Table 7
Analyzed results using Carson model of MF with dextran (T20), H = 17 mT.

Solid content, c_s (wt.%)	5.00	10.0	15.0	25.0	35.0
Carson's viscosity, η_c (mPa s)	0.380	0.410	4.59	0.870	12.5
Carson's yield stress, τ_c (Pa)	4.13	6.13	2.74	0.970	1.53
Correlation coefficient (%)	90.2	90.9	96.1	87.0	93.2

Table 8
Analyzed results using Herschel–Bulkley model of MF with dextran (T20), H = 17 mT.

Solid content, c_s (wt.%)	5.00	10.0	15.0	25.0	35.0
Herschel–Bulkley coefficient, k	5.19	8.04	13.2	16.7	23.7
Yield stress, τ_0 (Pa)	1.35	1.68	2.35	4.66	5.46
Shear thinning exponent, n	0.820	0.850	0.850	0.880	0.860
Correlation coefficient (%)	98.9	99.9	95.2	97.0	96.2

By comparing the Bingham, Carson and Herschel–Bulkley equations with the experimental results, it could be found that the Bingham constitutive equation is not recommended since it does not take account of the shear-thinning effect. On the other hand, the difference between the Herschel–Bulkley equation and the experimental results is the least. Therefore, the Herschel–Bulkley equation is recommended as the suitable constitutive equation for MFs with and without an external magnetic field.

From Table 5, one can see that there is a yield stress threshold when there is no magnetic field, even though it is small. The yield stress increases linearly with the increasing solid content. This is in accordance with the results of our published article [30]. When an external magnetic field is applied, the yield stress becomes comparatively high and increases with the increasing solid content, just as the case in Table 8. So, for the MFs prepared in the present

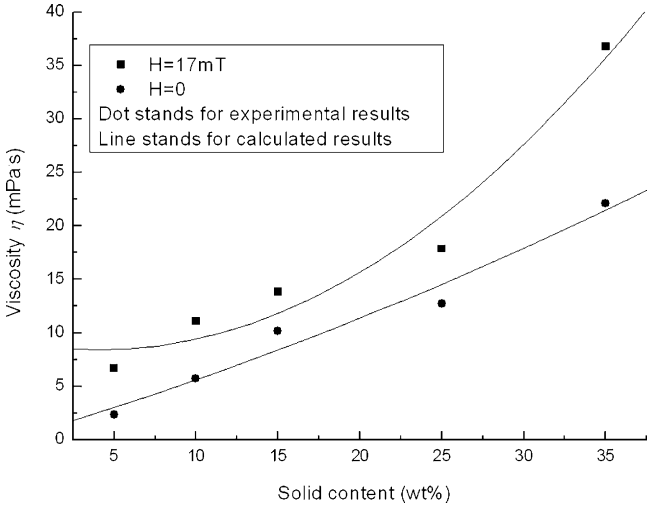

Fig. 11. Viscosity versus solid content of MF (stabilized by T20 dextran) with and without magnetic field (T = 23.5 °C) based on the theoretical calculation and experiment.

investigation, the Herschel–Bulkley model should be modified to:

$$\tau = \tau_0 + \tau_{H_0} + k\gamma^n \quad (1)$$

where, τ_0 is the yield stress threshold without magnetic field which is related to the solid content, and τ_{H_0} is the additional yield stress threshold under magnetic field which is determined by both the magnetic property of MF and magnetic field intensity. The τ_{H_0}, which takes the following form, is derived in detail in reference [30]:

$$\tau_{H_0} = \frac{r_0^3 c_s \mu^0 r \chi^2 H_0^2 \cos^2\gamma \sin\gamma}{12(r_0 + l)^3[\rho_s(1 - c_s) + c_s](2r + \delta)} \quad (2)$$

The results calculated using Eq. (2) are shown in Fig. 11. It is found that the theoretical model for the yield stress threshold is in accordance with the experimental results.

4. Conclusions

By chemical synthesis and physical characterization in the present investigation, the following conclusions can be drawn. (1) Magnetite/dextran nanocomposite was prepared through a two-step method. This route consists of the first introduction of amino-silane group onto the magnetite surface and the second coupling of oxidized dextran via formation of Schiff's base. (2) The molecular weight of dextran plays an important role on the size, morphology, coating efficiency, and magnetic property of MNPs/aggregates. (3) The surface modification of MNPs with dextran is propitious to the stability of MF. The viscosity of MF increases with the increasing molecular weight of dextran. (4) An external magnetic field can enhance the interaction among MNPs, therefore, the viscosity of MF increases under the external magnetic field. The magnetic field could also rearrange the MNPs, leading to the formation of orderly microstructures. When there is no magnetic field, the viscosity of MF increases linearly with the solid content. If an external magnetic field is applied, the viscosity increases quadratically with the solid content. (5) Our previously proposed constitutive equation is recommended for describing the rheological property of the water-based MF containing dextran-coated MNPs.

Acknowledgments

The project was supported by the National Natural Science Foundation of China (NNSFC, Nos. 20876100 and 20736004), the National Basic Research Program of China (Profile of 973 Program, No. 2009CB219904), the State Key Lab. of Multi-phase Complex Systems at the Institute of Process Engineering of the Chinese Academy of Sciences (No. 2006-5), the Key Lab. of Organic Synthesis of Jiangsu Prov. and R&D Foundation of Nanjing Medical Univ. (NY0586).

References

[1] S.M. Moghimi, A.C.H. Hunter, J.C. Murray, Long-circulating and target-specific nanoparticles: theory to practice, Pharm. Rev. 53 (2001) 283–318.
[2] S.L. Tie, Y.Q. Lin, H.C. Lee, Y.S. Bae, C.H. Lee, Amino acid-coated nano-sized magnetite particles prepared by two-step transformation, Colloids Surf. A 273 (2006) 75–83.
[3] J.M. Wilkinson, Nanotechnology applications in medicine, Med. Device Technol. 14 (2003) 29–31.
[4] J. Panyam, V. Labhasetwar, Biodegradable nanoparticles for drug and gene delivery to cells and tissue, Adv. Drug Del. Rev. 55 (2003) 329–347.
[5] U. Schwertmann, R.M. Cornell, Iron oxides in the laboratory: preparation and characterization, VCH, Weinheim, Cambridge, 1991.
[6] C. Wilhelm, C. Billotey, J. Roger, J.N. Pons, J.-C. Bacri, F. Gazeau, Intracellular uptake of anionic superparamagnetic nanoparticles as a function of their surface coating, Biomaterials 24 (2003) 1001–1011.
[7] X.Q. Liu, J.M. Xing, Y.P. Guan, G.B. Shan, H.Z. Liu, Synthesis of amino-silane modified superparamagnetic silica supports and their use for protein immobilization, Colloids Surf. A 238 (2004) 127–131.
[8] R.Y. Hong, B. Feng, L.L. Chen, G.H. Liu, H.Z. Li, Y. Zheng, D.G. Wei, Synthesis, characterization and MRI application of dextran-coated Fe_3O_4 magnetic nanoparticles, Biochem. Eng. J. 42 (2008) 290–300.
[9] R. Hiergeist, W. Andrä, N. Buske, R. Hergt, I. Hilger, U. Richter, W. Kaiser, Application of magnetite ferrofluids for hyperthermia, J. Magn. Magn. Mater. 201 (1999) 420–422.
[10] A.P. Astalan, F. Ahrentorp, C. Johansson, K. Larsson, A. Krozer, Biomolecular reactions studied using changes in Brownian rotation dynamics of magnetic particles, Biosens. Bioelectron. 19 (2004) 945–951.
[11] S. Odenbach, Ferrofluids-magnetically controlled suspensions, Colloids Surf. A 217 (2003) 171–178.
[12] Y.H. Deng, C.C. Wang, J.H. Hu, W.L. Yang, S.K. Fu, Investigation of formation of silica-coated magnetite nanoparticles via sol-gel approach, Colloids Surf. A 262 (2005) 87–93.
[13] J. Yu, C.W. Lee, S.S. Im, J.S. Lee, Structure and magnetic properties of SiO_2 coated Fe_2O_3 nanoparticles synthesized by chemical vapor condensation process, Rev. Adv. Mater. Sci. 4 (2003) 55–59.
[14] L. Shen, P.E. Laibinis, T.A. Hatton, Bilayer surfactant stabilized magnetic fluids: synthesis and interactions at interfaces, Langmuir 15 (1999) 447–453.
[15] C.E. Astete, C. Kumar, C.M. Sabliov, Size control of poly(d,l-lactide-co-glycolide) and poly(d,l-lactide-co-glycolide)-magnetite nanoparticles synthesized by emulsion evaporation technique, Colloids Surf. A 299 (2007) 209–216.
[16] A.K. Gupta, A.S.G. Curtis, Surface modified superparamagnetic nanoparticles for drug delivery: interaction studies with human fibroblasts in culture, J. Mater. Sci. Mater. Med. 15 (2004) 493–496.
[17] R.A. Wassel, B. Grady, R.D. Kopke, K.J. Dormer, Dispersion of super paramagnetic iron oxide nanoparticles in poly(d,l-lactide-co-glycolide) microparticles, Colloids Surf. A 292 (2007) 125–130.
[18] Y. Zhou, S.X. Wang, B.J. Ding, Z.M. Yang, Modification of magnetite nanoparticles via surface-initiated atom transfer radical polymerization (ATRP), Chem. Eng. J. 138 (2008) 578–585.
[19] R.K. Gilchrist, R. Medal, W.D. Shorey, R.C. Hanselman, J.C. Parrot, C.B. Taylor, Selective inductive heating of lymph nodes, Ann. Surg. 146 (1957) 596–606.
[20] G. Pitarresi, F.S. Palumbo, G. Giammona, M.A. Casadei, F.M. Moracci, Biodegradable hydrogels obtained by photocrosslinking of dextran and polyaspartamide derivatives, Biomaterials 24 (2003) 4301–4313.
[21] L. Vekas, D. Bica, I. Potencz, D. Gheorghe, O. Balau, M. Rasa, Concentration and composition dependence of rheological and magnetorheological properties of some magnetic fluids, Progr. Colloid Polym. Sci. 117 (2001) 104–109.
[22] G. Bossis, O. Volkova, S. Lacis, A. Meunier, Fluids, Structures and Rheology, Magnetorheology, Springer, Berlin/Heidelberg, 2002.
[23] C.F. Welch, G.D. Rose, D. Malotky, S.T. Eckersley, Rheology of high internal phase emulsions, Langmuir 22 (2006) 1544–1550.
[24] X. Qin, M.R. Thompson, A.N. Hrymak, Rheological comparison of chemical and physical blowing agents in a thermoplastic polyolefin, Ind. Eng. Chem. Res. 45 (2006) 2734–2740.
[25] H. See, Field dependence of the response of a magnetorheological suspension under steady shear flow and squeezing flow, Rheol. Acta 42 (2003) 86–92.
[26] S. Odenbach, H. Stòrk, Shear dependence of field-induced contributions to the viscosity of magnetic fluids at low shear rates, J. Magn. Magn. Mater. 183 (1998) 188–194.
[27] R.Y. Hong, Z.Q. Ren, S.Z. Zhang, J.M. Ding, H.Z. Li, Numerical simulation and experimental verification of silicone oil flow over magnetic fluid under applied magnetic field, China Particuol. 5 (2007) 93–102.
[28] J. Vicente, M.T. Lòpez, J.D.G. Durán, F.C. González, Shear flow behavior of confined magnetorheological fluids at low magnetic field strengths, Rheol. Acta 44 (2004) 94–103.
[29] R.Y. Hong, S.Z. Zhang, Y.P. Han, H.Z. Li, J. Ding, Y. Zheng, Preparation, characterization and application of bilayer surfactant-stabilized ferrofluids, Powder Technol. 170 (2006) 1–11.
[30] R.Y. Hong, Z.Q. Ren, Y.P. Han, H.Z. Li, Y. Zheng, J. Ding, Rheological properties of water-based Fe_3O_4 ferrofluids, Chem. Eng. Sci. 62 (2007) 5912–5924.
[31] L. Betancor, M. Fuentes, G. Dellamora-Ortiz, F. López-Gallego, A. Hidalgo, N. Alonso-Morales, C. Mateo, J.M. Guisán, R. Fernández-Lafuente, Dextran aldehyde coating of glucose oxidase immobilized on magnetic nanoparticles prevents its inactivation by gas bubbles, J. Mol. Catal. B-Enzym. 32 (2005) 97–101.
[32] R.Y. Hong, T.T. Pan, H.Z. Li, Microwave synthesis of magnetic Fe_3O_4 nanoparticles used as a precursor of nanocomposites and ferrofluids, J. Magn. Magn. Mater. 303 (2006) 60–68.
[33] X. Hong, W. Guo, H. Yuan, J. Li, Y.M. Liu, L. Ma, Y.B. Bai, T.J. Li, Periodate oxidation of nanoscaled magnetic dextran composites, J. Magn. Magn. Mater. 269 (2004) 95–100.
[34] J. Battersby, R. Clark, W. Hancock, E. Puchulu-Campanella, N. Haggarty, D. Poll, D. Harding, Sustained release of recombinant human growth hormone from dextran via hydrolysis of an imine bond, J. Control. Release 42 (1996) 143–156.

[35] J.M. Guisan, V. Rodriguez, C.M. Rosell, G. Soler, A. Bastida, R. Fernández-Lafuente, E. García-Junceda, Methods in biotechnology, in: G. Bickerstaff (Ed.), Immobilization of Enzymes and Cells, vol. 1, Humana Press, Totowa, NJ, 1997, p. 261.
[36] J. Giria, S.G. Thakurtaa, J. Bellareb, A.K. Nigamc, D. Bahadur, Preparation and characterization of phospholipid stabilized uniform sized magnetite nanoparticles, J. Magn. Magn. Mater. 293 (2005) 62–68.
[37] X.Q. Xu, H. Shen, J.R. Xu, J. Xu, X.J. Li, X.M. Xiong, Core-shell structure and magnetic properties of magnetite magnetic fluids stabilized with dextran, Appl. Surf. Sci. 252 (2005) 494–500.
[38] R.Y. Hong, J.H. Li, H.Z. Li, J. Ding, Y. Zheng, D.G. Wei, Synthesis of Fe_3O_4 nanoparticles without inert gas protection used as precursors of magnetic fluids, J. Magn. Magn. Mater. 320 (2008) 1605–1614.